Proceedings of
ASME TURBOEXPO 2000
May 8-11, 2000, Munich Germany

2000-GT-281

FLOW AND HEAT TRANSFER IN A ROTATING CAVITY WITH A STATIONARY STEPPED CASING

Abdul A Jaafar
Department of Mechanical Engineering
University of Bath, Bath BA2 7AY, UK

Fariborz Motallebi
Engineering Department
Queen Mary & Westfield College, London, UK

Michael Wilson
Department of Mechanical Engineering
University of Bath, Bath BA2 7AY, UK

J Michael Owen
Department of Mechanical Engineering
University of Bath, Bath BA2 7AY, UK

ABSTRACT

In this paper, new experimental results are presented for the flow in a co-rotating disc system with a rotating inner cylinder and a stationary stepped outer casing. The configuration is based on a turbine disc-cooling system used in a gas turbine engine. One of the rotating discs can be heated, and cooling air is introduced through discrete holes angled inward at the periphery of this disc. The cooling air leaves the system through axial clearances between the discs and the outer casing. Some features of computed flows, and both measured and computed heat transfer, were reported previously for this system. New velocity measurements, obtained using Laser Doppler Anemometry, are compared with results from axisymmetric, steady, turbulent flow computations obtained using a low-Reynolds-number k-ε turbulence model.

The measurements and computations show that the tangential component of velocity is invariant with axial location in much of the cavity, and the data suggest that Rankine (combined free and forced) vortex flow occurs. The computations fail to reproduce this behaviour, and there are differences between measured and computed details of secondary flow recirculations. Possible reasons for these discrepancies, and their importance for the prediction of associated heat transfer, are discussed.

1 INTRODUCTION

Gan et al (1996) and Mirzaee et al (1998) studied the flow and heat transfer in a rotating cavity with a peripheral flow of cooling air through a flat, stationary outer casing. Shear at the stationary casing gave rise to symmetric twin recirculations for the secondary flow (in the axial-radial plane) in the outer part of the cavity. Cooling air, introduced with zero swirl at the mid-axial plane of the casing and directed radially inward, increased the inward penetration of the recirculations. For sufficiently high flow rates, the recirculations reached a rotating inner cylinder (or hub) at $x = r / b = 0.5$. LDA measurements were made in this system for both radial and tangential velocity distributions, and corresponding computations were carried out assuming axisymmetric, steady flow and using the Launder-Sharma (1974) low Reynolds-number k-ε turbulence model. The agreement between computed and measured radial velocity distributions was reasonable, although the inward penetration of the cooling air was overpredicted. Radial distributions of tangential velocity (measured outside the boundary layers on the rotating discs) followed a Rankine (combined free and forced) vortex structure. At the highest cooling-air flow-rates studied, the tangential velocity distribution was close to free-vortex behaviour, and the agreement between computations and data was good. (For cases with no superposed cooling flow, the agreement was poor.) Computed and measured Nusselt numbers were also in reasonable agreement, provided the combined effects of conduction, through a disc not insulated in the experiment, and of surface-to-surface radiation were included in the computational model. In general, measured Nusselt numbers were under-predicted, but the effects of rotational Reynolds number and cooling-air flow rate were reproduced correctly.

Mirzaee et al (1999) reported measurements and computations of heat transfer for a similar rotating cavity with air introduced through holes near the periphery of a heated rotating disc (thus imparting swirl to the incoming flow). A "stepped" stationary casing of square cross-section was used, and (as above) the superposed flow left the system through axial clearances at the outer casing. The geometry of this cavity is shown in Fig. 1. The computations suggested that the flow structure depended strongly on the turbulent flow parameter, λ_T, which is defined in the nomenclature and which combines the effects of rotational speed and flow-rate (see Mirzaee et al (1999)). At low values of λ_T, the secondary flow was confined mainly to the outer part of the system, with recirculations driven by the discs and the surfaces of the square-sectioned casing, as shown in Fig. 2a. (The computed flow structure is discussed in more detail below). At higher values of λ_T, there was greater inward penetration of the swirling cooling-air. Measured velocity distributions were not available, however measured

values of Nusselt number were mostly well-predicted. The parametric variation of Nu with rotational Reynolds number and cooling-air flow-rate was also reproduced correctly.

The object of the present study is to investigate the flow and heat transfer in the rotating cavity with a stepped casing so as to provide data and insight for the designer. Details of the experimental study and the associated computational model, both of which are directly related to earlier work, are given in Section 2 and Section 3 respectively. Comparisons are made in Section 4 between computed and measured distributions of radial and tangential velocity; the latter are used to provide information on the possible inlet conditions (which were not measured directly) for the flow through the rotating holes in the disc. The effect of modified inlet boundary conditions on previously-reported comparisons between computed and measured heat transfer are also discussed in Section 4. Conclusions appear in Section 5.

NOMENCLATURE

a, b	inner, outer radius of cavity
c	inlet swirl ratio (= $(V_\phi / \Omega r)_i$)
C_w	nondimensional mass flow rate (= $m_i / \mu b$)
G	gap ratio (= s / b)
k	turbulent kinetic energy, thermal conductivity
m	mass flow rate
Nu	Nusselt number (= $qr/k(T_s - T_{ref})$)
q	heat flux from disc to air
r	radial coordinate
Re_ϕ	rotational Reynolds number (= $\rho\Omega b^2/\mu$)
s	axial gap between discs
T	temperature
V_r, V_ϕ	time-averaged velocities in r,ϕ directions
x	nondimensional radius (= r / b)
z	axial coordinate measured from upstream disc
Γ	ratio of outlet flow rates (= m_c / m_d)
ε	turbulent energy dissipation rate
λ_T	turbulent flow parameter (= $C_w Re_\phi^{-0.8}$)
μ	dynamic viscosity
ρ	density
ϕ	tangential coordinate
Ω	angular speed of discs

Subscripts

c	central clearance
d	downstream clearance
eff	effective value
i	inlet value
s	upstream (heated) disc surface
ref	reference value

2 EXPERIMENTAL APPARATUS

2.1 Rotating-Disc Rig

The rig used for the velocity measurements reported here was the same as that described by Mirzaee et al (1999) for an experimental

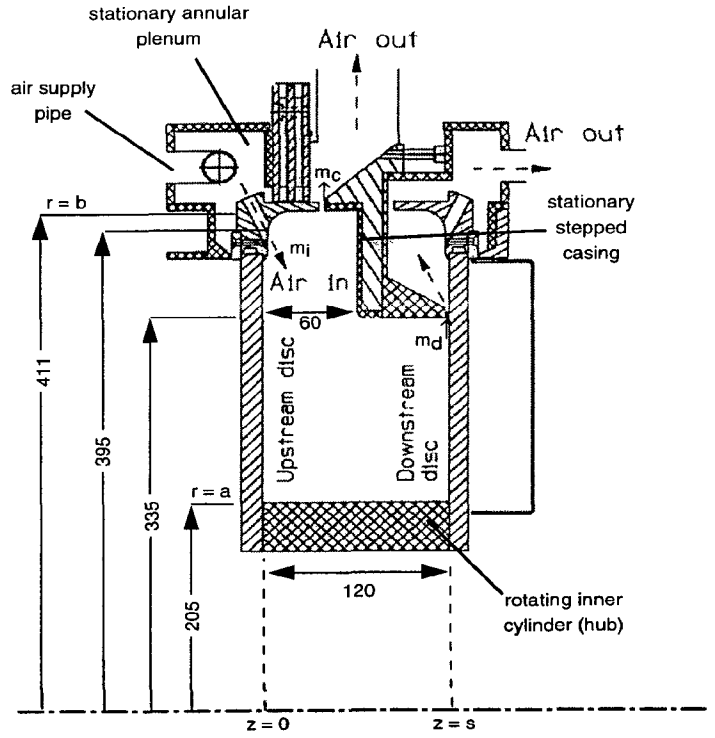

Fig. 1 Schematic diagram of experimental rig for the rotating cavity with a stationary stepped casing (not to scale, main dimensions given in mm)

study, which was restricted to heat transfer only. The geometry and main dimensions for the rig are shown in Fig. 1. Air entered the cavity through 74 evenly-distributed holes in a nozzle-ring attached to the upstream rotating disc. Each hole was of 8.6-mm diameter and was angled inward at 24° to the radial direction. The air was supplied to the holes from a stationary annular plenum, itself supplied from six tubes oriented with their outlets tangential to the nozzle ring (in order to reduce the torque required to rotate the discs). Mirzaee et al assumed that the air entering the cavity through the rotating holes was in solid-body rotation at the same speed as the disc; this corresponds to c = 1, where c = $(V_\phi/\Omega r)_i$ is the ratio of the tangential speed of the air to that of the disc at the inlet radius. This assumption was not confirmed experimentally, and there are indications from the measured data that solid-body rotation may not have occurred, as described below. (The tangential velocity of the air entering the stationary plenum increases with increasing flow-rate, so that the assumed condition c = 1 is likely to be more realistic for the highest flow-rate cases considered.) The rotational speed of the cavity, which was kept sensibly constant by a thyristor-controlled electric motor, was measured, with an uncertainty of ±1 rev/min, by an electronic tachometer.

As shown in Fig 1, air could leave the cavity through two clearances: a "central clearance", between the upstream nozzle ring and the stationary casing and a "downstream clearance" between the downstream disc and the casing. For the results discussed below, the flow was split equally between the two outlets, i.e. $m_c = m_d = 0.5\ m_i$.

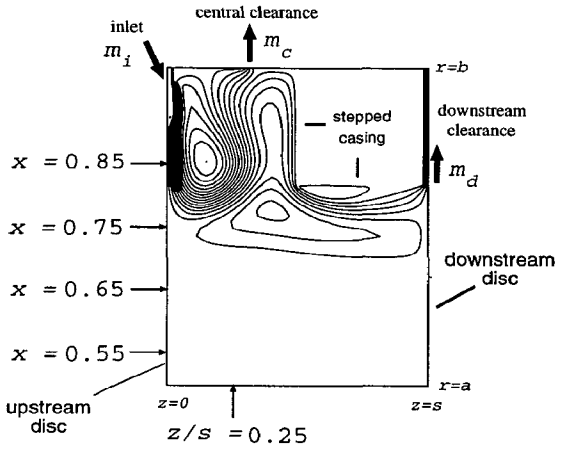

a) Computational model showing selected measurement locations and computed streamlines ($Re_\phi = 9.39x10^5$, $C_W = -24{,}000$ ($|\lambda_T| = 0.4$) , c = 1)

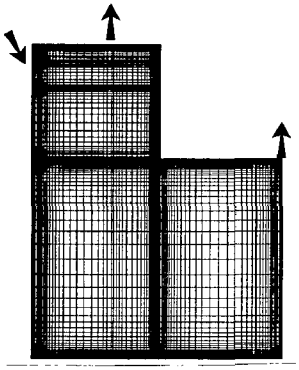

b) 147 x 131 radial x axial grid

Fig. 2 Details of the computational model

The mass flow rates, m_i (the flow rate entering the cavity), m_c and m_d were measured, using orifice plates made to British Standards BS1042, with an uncertainty of ±3%. The typical difference between the mass flow into and out of the rig was less than 0.5%. (The accuracy of the individual flow rates depended upon the effectiveness of the seals, but the leakage between the air entering and leaving the system through the central clearance was minimised by pressurising the seal on the nozzle ring.)

The laser Doppler anemometry (LDA) measurements required the replacement of the instrumented steel upstream disc (see Fig. 1), used for the earlier heat transfer work of Mirzaee et al (1999), by a new steel disc having eight, circular, perspex (acrylic plastic) windows. The windows provided optical access over part of the disc surface: the centre of the windows was located at a radius of 280.5 mm, and the viewing diameter of each window was 161 mm. Thus, the radial extent of the cavity that could be viewed was between r = 200 and r = 361 mm, corresponding to x = 0.487 and x = 0.878 (where b = 411 mm). The maximum percentage of time, per revolution of the disc, that could be used for LDA measurements was 73% at x = 0.68; for smaller or larger values of x, the percentage was less.

Relevant details of the heat transfer measurements, obtained by Mirzaee et al as part of a separate investigation, are given in Section 3 in connection with the computational model.

2.2 LDA Velocity Measurements

The LDA system used was very similar to that described by Gan et al (1996), and only salient details are given here. The system used a 4W Spectra-Physics argon-ion laser, the beam of which was transmitted to the optics through a fibre-optics cable with an efficiency of around 50%. The TSI optics, which were configured in a single-component back-scatter mode, were mounted on an x-y traversing table, allowing movement in the radial and axial directions. By turning the transmitting optics through 90°, it was possible to measure either the radial or the tangential component of velocity. The transmitting optics included a Bragg-cell which allowed frequency shifts of up to 40 MHz, and the beam spacing was 50 mm which, with a 250 mm focal length lens, produced an optical probe volume around 1.4 mm long and 0.14 mm diameter.

The Doppler signal from the receiving optics was processed by a TSI IFA-750 burst correlator, which could handle frequencies up to 90 MHz with signal-to-noise ratios (SNRs) as low as –5 dB. The measurements were made through windows in the steel disc, as described above, which meant that the light beams were interrupted, and an opto-electronic switch, synchronised with the disc rotation, was used to trigger the signals. This reduced significantly the rate of data processed by the correlator.

For velocity measurements in the cavity, the air upstream of the rig was seeded with micron-sized oil particles. Oil deposition on the rotating surfaces meant that the perspex window had to be frequently removed for cleaning.

The accuracy of the velocity measurements was confirmed by locating the probe volume in the rotating windows. The measured tangential component of velocity, V_ϕ, was typically found to be within 1% of Ωr, where Ω was the measured angular speed of the disc. By turning the optics through 90°, the radial direction was found precisely by fine adjustment until the Doppler signal was zero. It is not easy to quantify the errors in $V_r/\Omega r$, but they are significantly less than 1%.

Axial distributions of V_r and V_ϕ were measured at five radial locations: x = 0.55, 0.6, 0.65, 0.7 and 0.75; the radial distributions of V_ϕ discussed below were measured at z/s = 0.25. These locations are illustrated in Fig. 2a, and measurements were made no closer than 5 mm to either disc (that is, z/s = 0.0417 and z/s = 0.958), due to flare from the solid surfaces.

2.3 Range of Nondimensional Parameters

Twelve different flow conditions were considered in the experimental study upon which this paper is based. Measurements were made at two rotational Reynolds numbers, $Re_\phi = 4.35 \times 10^5$ and $Re_\phi = 9.39 \times 10^5$, the nondimensional flow rates studied were $C_W = -7{,}000$, $-13{,}000$ and $-24{,}000$ approx. (by convention, the negative sign is used to indicate radial inflow), and the Γ values were 0.15, 0.5 and 1. The discussion of computed and measured results

given below relates to four cases, each having $\Gamma = 1$, these being at the two higher flow rates at each rotational Reynolds number.

3 COMPUTATIONAL MODEL

The computational model for incompressible flow and heat transfer for the rotating cavity shown in Fig. 1 was developed by Mirzaee et al (1999) using an axisymmetric, steady flow research code and the Launder-Sharma low-Reynolds-number k-ε turbulence model. As described by Mirzaee et al, a 147 x 131 radial x axial grid was used (Fig. 2b), contracted to the solid surfaces in order to satisfy the demanding requirements of the turbulence model. The stepped casing was represented as a block obstruction within the cylindrical-polar mesh, and the angled inlet nozzles were modelled as an equivalent-area annular slot having the same centreline radius at the disc surface. Appropriate axial and radial velocity components were prescribed at the inlet, having been deduced from the known inlet mass flow rate in the corresponding experiment. Different values of tangential velocity V_ϕ were imposed at the inlet, in separate computations, in order to study the effect of inlet swirl ratio c on the computed results. Uniform radial velocity was imposed at the two outlet boundaries to meet the $\Gamma = 1$ (equal flow-rate) condition, and zero normal derivative conditions were imposed for other solution variables at oulet. Further details are given by Mirzaee et al.

Mirzaee et al also discussed in detail the thermal boundary conditions used for the computations, and the uncertainties surrounding these in the experiments. Identical modelling practices have been used in the work reported below, the most important being the use of a conduction assumption to compute the unknown temperature of the unheated downstream disc. Temperatures, measured using thermocouples, were used to prescribe a temperature distribution for the heated upstream disc, while the inner casing at $r = a$ and the stepped outer casing were insulated and assumed to be adiabatic.

The total heat transfer rate, measured by fluxmeters located on the heated disc, included a contribution due to radiation. A surface-to-surface radiation model was used to compute the radiative heat transfer (based on predicted surface temperatures) which was added to the computed convective heat fluxes. This enabled consistent comparisons to be made between computed and measured values of Nusselt number for the heated disc. Again, further details of the procedure are given by Mirzaee et al, and results relevant to the present work are presented in Section 4.4.

4 RESULTS AND DISCUSSION

4.1 Computed Secondary Flow Streamlines

Fig. 3 shows the computed streamlines for four combinations of Re_ϕ and C_W; the direction of circulation can be deduced by referring to Fig. 2a for the flow directions. For each combination, computations were carried out for three values of c, the inlet swirl ratio: $c = 1$, $c = c_{eff}$ and $c = 0$. The value $c = 1$ corresponds to the case where the air enters the system with a tangential component of velocity equal to that of the rotating discs; this was the value of c assumed by Mirzaee et al (1999). The value $c = c_{eff}$, an effective swirl ratio, was based on the measured velocities, as described below ($c_{eff} > 2/3$ for three out of the four cases in Fig. 3). The value $c = 0$ corresponds to the case where the air enters the system without swirl; it is physically unrealistic but serves to provide a datum.

For $c = 1$, the computed streamlines of Mirzaee et al showed that, for any combination of Re_ϕ and C_W, the flow structure depends principally upon the value of λ_T. For $\lambda_T = -0.4$, Fig. 3a and Fig. 3d show that, for a fixed value of c, the flow structures are similar. In general, the flow depends strongly on λ_T and c. (The different flow structures obtained were illustrated schematically by Mirzaee et al.)

For the $c = 1$ cases, the air enters the cavity with a radial inflow on the rotating disc and there is outflow at the central clearance. This creates anti-clockwise and clockwise circulations near, respectively, the upstream disc and the radial surface of the stationary casing, and the size of the recirculation regions increases as $|\lambda_T|$ increases. There is axial flow along the surface of the stepped casing toward the downstream clearance. Similar patterns occur for $c = c_{eff}$. For $c = 0$, there is less swirl in the cavity. The "disc pumping effect" suppresses the radial inflow, and weakens the anti-clockwise circulation, near the rotating disc. (There is also an increased region of flow separation at the axial surface of the stepped casing at each condition.)

4.2 Tangential velocity distributions

Measured tangential velocities, taken at $z/s = 0.25$, are shown in Fig. 4 in comparison with the results of computations for each of the three different inlet swirl assumptions. The distributions are plotted against both non-dimensional radius x (= r/b, see Fig. 2) and x^{-2}. In the latter representation a straight line indicates a combined free and forced (or Rankine) vortex (see Owen and Rogers (1995) and Gan et al (1996)), for which:

$$\frac{V_\phi}{\Omega r} = Ax^{-2} + B$$

where A and B are constants; the case where $B = 0$ corresponds to a free vortex.

The "Rankine-vortex lines" drawn through the measured data in Fig. 4a-d (ii) were used to calculate the values of the effective swirl ratio, c_{eff}, given in Fig. 3, as the value of $V_\phi/\Omega r$ at $x = 1$ for each case. These will not correspond to the true inlet swirl ratios, due to the very significant mixing near the inlet (as illustrated in Fig. 3), however in the absence of detailed information on inlet conditions in the experiment this procedure allows the importance of this parameter to be investigated.

The results given in Fig. 4a show that, at $Re_\phi = 4.35 \times 10^5$ and $C_W = -13{,}000$ ($|\lambda_T| = 0.4$), computed values of tangential velocity are considerably higher than those measured, except for the result for $c = 0$. In this and subsequent figures, the $c = 0$ result is shown mainly to illustrate the range of variation of the computed results for $0 \le c \le 1$. The condition $c = 0$ is not believed to be a realistic description of the flow at inlet in any of these cases, and these results will not be considered in detail. The computed results for $c = 1$ and $c = c_{eff}$ in Fig. 4a are similar in character, with the peak value of $V_\phi/\Omega r$ occurring further radially inward for the case with lower inlet swirl. A peak in $V_\phi/\Omega r$ also occurs in the measured data for $x > 0.8$; the computations fail to reproduce this feature accurately. Further remarks on these discrepancies will be made below.

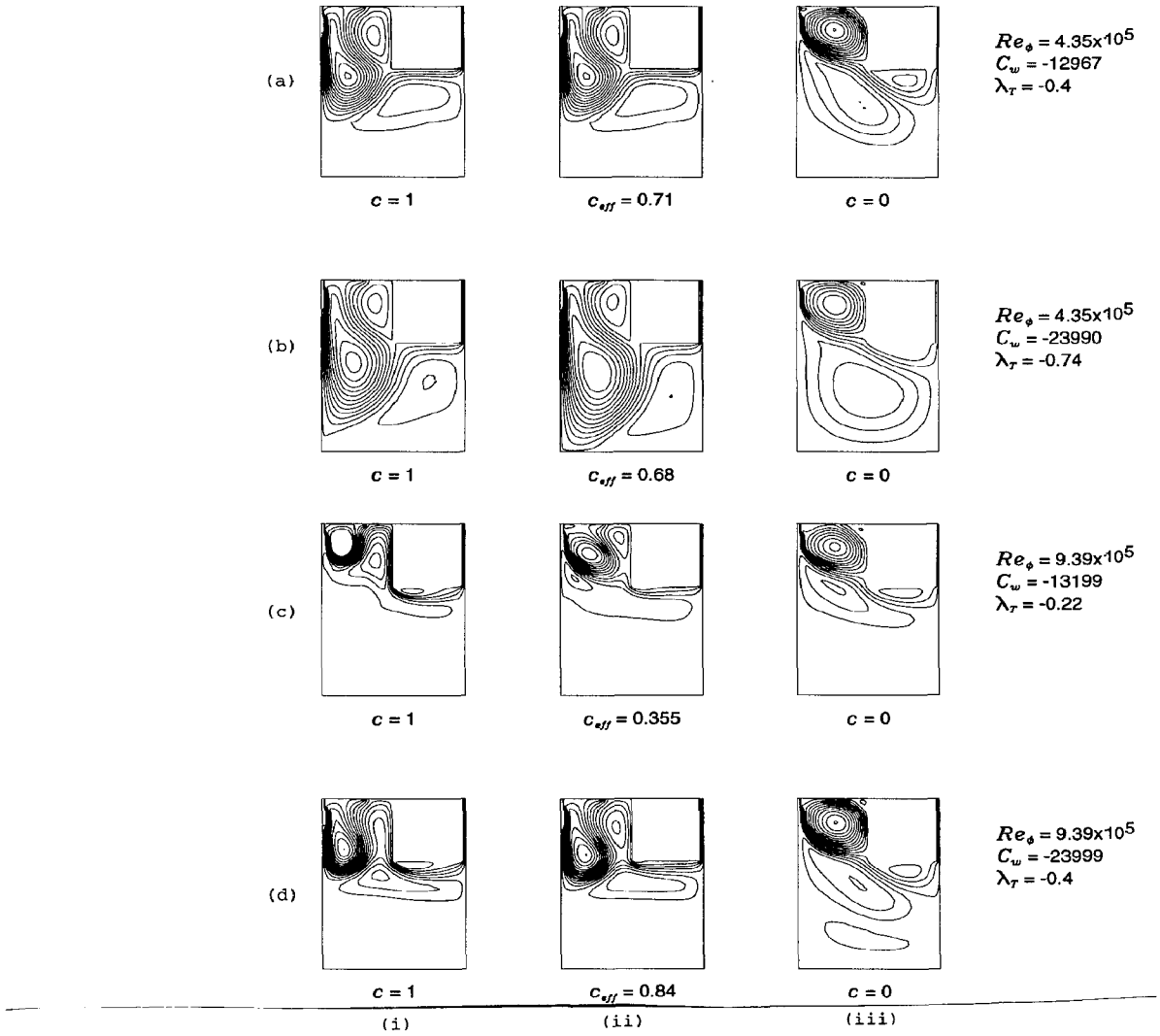

Fig. 3 Computed secondary flow streamlines, showing the effect of inlet swirl ratio c

Results for $Re_\phi = 4.35x10^5$ and $C_W = -24{,}000$ ($|\lambda_T| = 0.74$) are shown in Fig. 4b. In this case the high flow rate, at comparatively low Reynolds number, gives rise to a measured flow structure in the outer part of the system which follows (approximately) a free vortex description for $x > 0.7$ approx.; further radially inward, forced vortex flow is observed with the air rotating faster than the discs ($V_\phi/\Omega r > 1$). The measured velocities in the outer part of the system are well predicted by the computations with $c_{eff} = 0.68$, however forced vortex flow in the inner region is not predicted.

Fig. 4c shows computed and measured results for a higher rotational Reynolds-number, $Re_\phi = 9.39x10^5$, than for those discussed above. The flow rate is $C_W = -13{,}000$, giving $|\lambda_T| = 0.22$. For this case, even the computations for $c = 0$ overpredict most of the measured velocities for $x > 0.65$ approx., suggesting that there are considerable inadequacies in the computational model used here in addition to the uncertainties surrounding the inlet conditions. The peak in the computed result for $c = c_{eff}$ partially reflects the measured behaviour at $x = 0.8$ approx., but the slope of the computed distribution is in very poor agreement with the more systematic behaviour indicated by the data (Fig. 4c(ii)). This discrepancy may be similar in origin to that discussed by Mirzaee et al (1998) for a rotating cavity with a flat stationary casing (and superposed flow with zero inlet swirl). Mirzaee et al obtained improved agreement with data in that work by including a Richardson-number-based correction to the dissipation equation in the Launder-Sharma k-ε turbulence model. This was not found to give the same degree of improvement for all of the conditions studied and so was not tested in the present work.

Fig. 4d shows computed and measured results for $Re_\phi = 9.39 \times 10^5$ and $C_W = -24{,}000$ ($|\lambda_T| = -0.4$). The λ_T value is the same as that for the lower Reynolds number case discussed above and shown in Fig. 4a. Broadly similar comments apply to the results shown in Fig. 4d, with the exception that computed tangential velocities are closer to the measured values in the inner part of the system ($x < 0.6$).

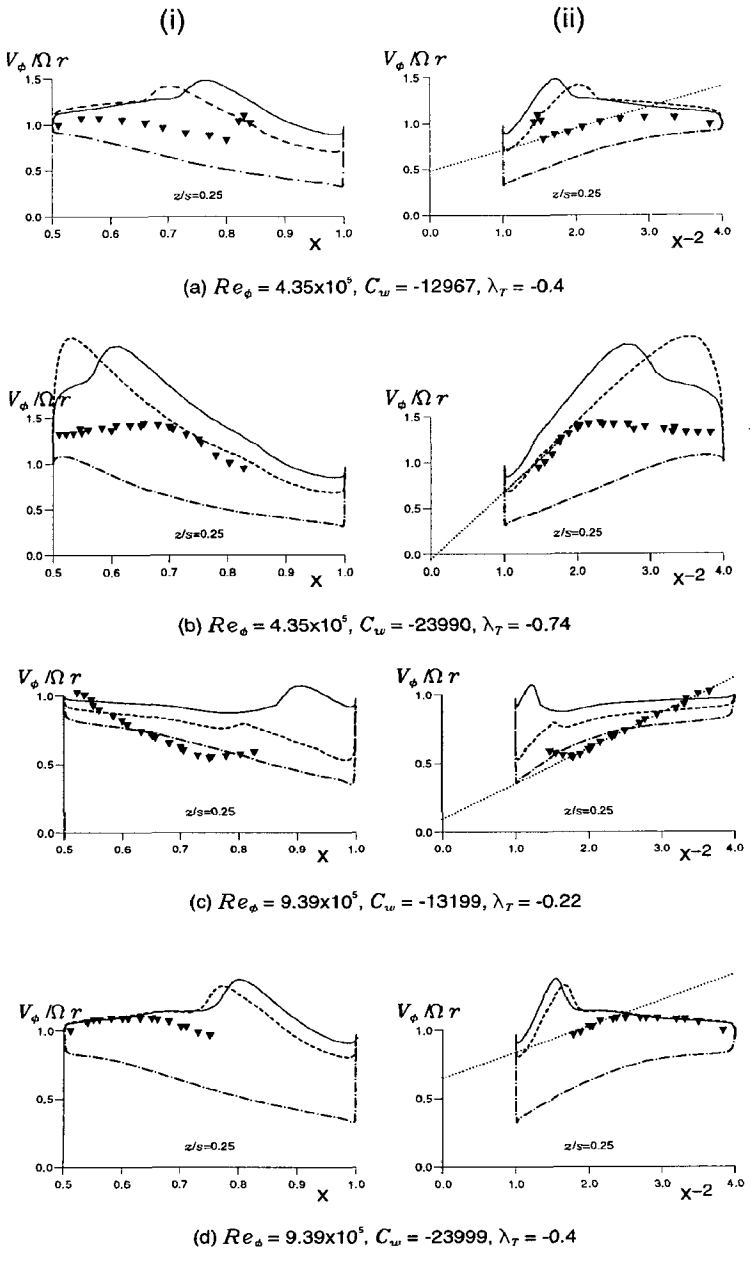

Fig. 4 Comparisons between computed and measured radial distributions of tangential velocity at z/s = 0.25

▼ measured
——— computed using c = 1
--------- computed using c = c_{eff}
– – – – computed using c = 0
--------- Rankine vortex line

The measured data are similar for the two Reynolds numbers in Fig. 5 but the computations show significant differences. In order to investigate the poor agreement, further computations were conducted for $Re_\phi = 4.35 \times 10^5$ using both a fully turbulent high-Reynolds-number k-ε model with wall-functions, and a high-Reynolds-number Reynolds stress model.

The Launder-Sharma model, used to obtain the computed results shown in Fig. 5, is able to represent transition from laminar to turbulent flow at low values of Re_ϕ. For example, the computations of Gan et al (1994) produced laminar flow at low Re_ϕ whereas their experimental data suggested that the flow was turbulent. For the computations considered here, at $Re_\phi = 4.35 \times 10^5$, the results from the two high-Reynolds-number models agreed closely with those for the Launder-Sharma model. This suggests that neither transition nor the turbulence model used is the cause of the problem, although a low-Reynolds-number stress model has not been tested.

Other investigators (see Herrero et al 1999) have found that the flow in a sealed rotating cavity with a flat stationary casing can be three-dimensional and unsteady. It is therefore possible that the flow in a rotating cavity with a stepped casing cannot be computed accurately by a steady axisymmetric solver regardless of the turbulence model used.

4.3 Axial Velocity Distributions

Axial distributions of radial velocity V_r and tangential velocity V_ϕ were measured for only one of the four cases discussed above. Fig. 6 shows the comparison between computed and measured velocity distributions for $Re_\phi = 9.39x10^5$, $C_W = -24{,}000$ ($|\lambda_T| = 0.4$). Computed results are shown for both c = 1 and c = c_{eff} (= 0.84); the results obtained for c = 0 are omitted.

Mirzaee et al discussed, for c = 1, the variation of computed axial velocity distributions with the parameter λ_T, including the case $|\lambda_T| = 0.4$. Fig. 6a shows that, for this value of λ_T, there is reasonable agreement between the measurements for V_r at x = 0.75 and the computed distribution for c = 1. Radial inflow is computed in the boundary layers on both rotating discs. At x = 0.70, the only significant radial flow for c = 1 is the inflow on the downstream disc. Virtually no radial flow is computed for x < 0.70, and this is consistent with the invariance of V_ϕ with z shown in Fig. 6b (in both measurements and computations) at these locations. (It should be noted that the maximum measured radial velocity at any radius is no greater than 5% of the speed of the disc at the same radius.) Fig. 6a shows that the most significant effect of the parameter c is that, for c = c_{eff}, there is more powerful radial inflow near the upstream disc than for c = 1. This radial flow appears to be significantly overpredicted for c = c_{eff} in comparison with the measurements at x = 0.75; at x = 0.70, however, the c = c_{eff} results are in better agreement with the data than the c = 1 prediction in the region where the measurements show $V_r > 0$. The computed secondary flow streamlines for these conditions, shown in Fig. 3d, illustrate that the anti-clockwise recirculation close to the upstream disc extends inward to around x = 0.75 (see also Fig. 2 for the case with c = 1); the inward penetration depends upon c, and this gives rise to the differences in results shown in Fig. 6a at this location.

Fig. 6b shows that there is no measured axial variation in tangential velocity at x = 0.75 or x = 0.70; the computations, however,

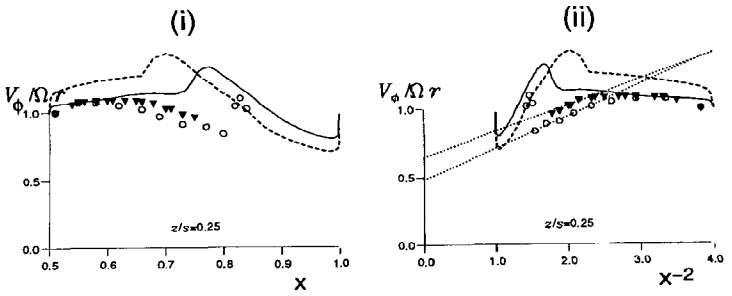

Fig. 5 Computed and measured radial distributions of tangential velocity for $|\lambda_T| = 0.4$, $c = c_{eff}$

$Re_\phi = 4.35 \times 10^5$: O measured ------- computed $c_{eff} = 0.71$
$Re_\phi = 9.39 \times 10^5$: ▼ measured —— computed $c_{eff} = 0.84$
--------- Rankine vortex line

show higher values of V_ϕ close to the upstream disc associated with the boundary layer fluid flowing radially inward from regions of higher angular momentum. It is possible that more rapid mixing occurs in the outer part of the system in the real flow than is predicted by these axisymmetric, steady computations.

4.4 Heat Transfer

Computed Nusselt number distributions on the heated disc were obtained using the same conduction assumptions for the unheated disc, and estimations of radiative heat transfer, described by Mirzaee et al (1999). Fig. 7a-d shows disc surface temperatures and computed Nu distributions for four of the cases previously studied by Mirzaee et al, at conditions very similar to those described above. (The reference temperature, T_{ref}, used in the definition of Nu was also given by Mirzaee et al for each of these cases based upon measured values. The velocity measurements described above were made in a subsequent study.) The main objective in the present work is to determine the effect of modified inlet swirl assumptions on the comparisons with Nu data reported by Mirzaee et al, for which c = 1 was used in the computations.

Fig. 7a(ii) shows that, at $Re_\phi = 3.93 \times 10^5$ and $C_W = -11{,}970$ ($|\lambda_T| = 0.4$), there is little difference between computed Nu results for c = 1 and $c = c_{eff}$ (= 0.71) at inlet. The computed result for c = 1 (in this and subsequent figures) is the same as that reported by Mirzaee et al. A computation using c = 0 is again included to indicate the range of variation of Nu with c. The corresponding temperature distributions computed for the unheated (downstream) disc are shown in Fig. 7a(i). There is little radial variation, and for c = 0 the disc temperature is cooler than for the other conditions. The same comments apply for subsequent cases, and the computed results for the unheated downstream disc will not be discussed further.

The relatively good agreement between computed and measured Nu shown in Fig. 7a(ii) is surprising, given the poor prediction of the flow structure suggested by the results in Fig. 3a. Similarly, the fair prediction of measured Nu data shown in Fig. 7b, for $Re_\phi = 4.31 \times 10^5$ and $C_W = -23{,}955$ ($|\lambda_T| = 0.745$), is not changed significantly through the use of $c_{eff} = 0.68$.

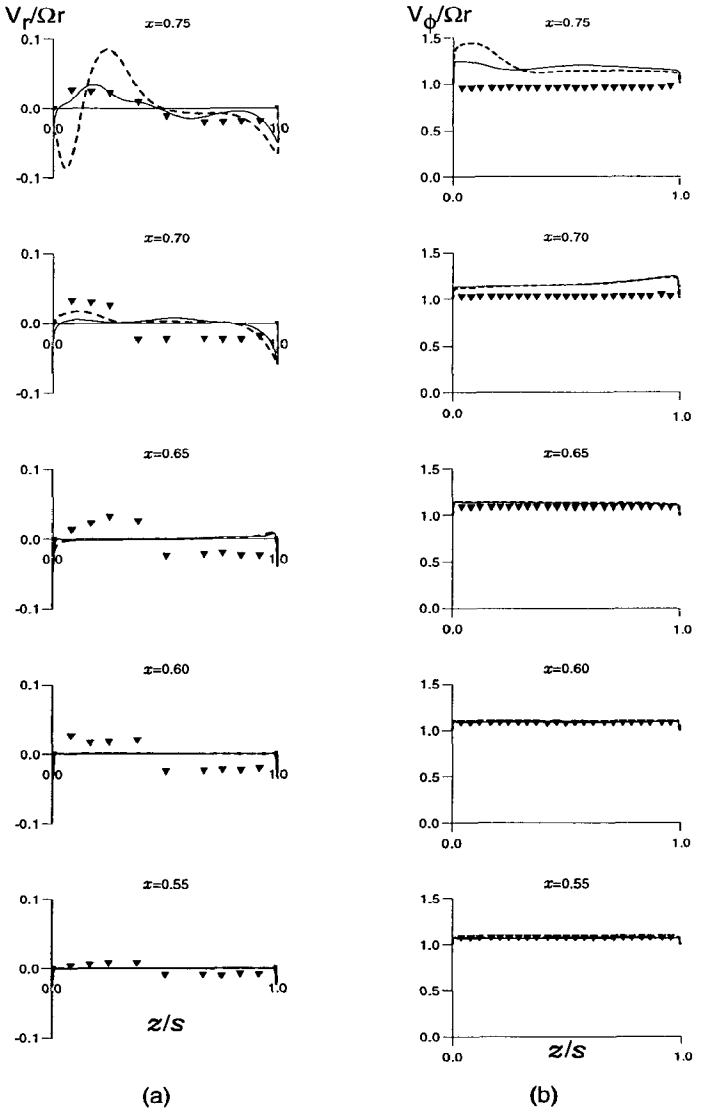

Fig. 6 Comparison between computed and measured axial distributions of velocity for $Re_\phi = 9.39 \times 10^5$, $C_W = -24{,}000$ ($|\lambda_T| = 0.4$):

(a) radial velocity and (b) tangential velocity

▼ measured
—— computed using c = 1
--------- computed using $c = c_{eff}$

For $Re_\phi = 7.75 \times 10^5$ and $C_W = -11{,}961$ ($|\lambda_T| = 0.233$), Fig. 7c(ii) shows that the computed results for $c = c_{eff}$ differ from those for c = 1 for x > 0.75 approx. Arguably, the c = 1 result is a better reflection of the measured rise in Nu at x = 0.85. In Fig. 7d(ii), the computed results for $c = c_{eff}$ overpredict the data at all of the measured locations.

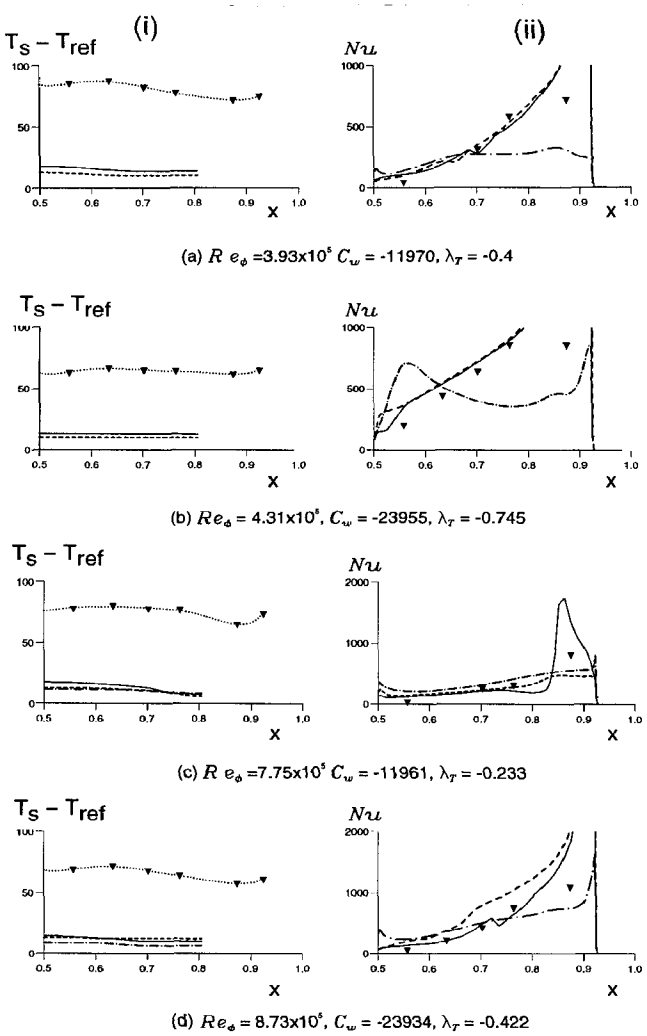

Fig. 7 Comparison between computed and measured temperatures and Nusselt numbers

▼ measured
——— computed using c = 1
--------- computed using c = c_{eff}
– - – - – computed using c = 0

5 CONCLUSIONS

This paper describes measured distributions of radial and tangential velocity for a rotating cavity with a stepped stationary outer casing and a peripheral flow of air, representing the cooling of a turbine disc in a gas-turbine engine. The measurements have been compared with previously reported computed flow structures, obtained in a prior experimental and computational study of heat transfer for the same system. The following main conclusions may be drawn from the new results presented here:

(i) measured radial distributions of tangential velocity show, in the main, that there is near solid-body rotation in the inner region of the cavity and combined free and forced (known as Rankine) vortex flow in the outer part of the system, due to the inwardly directed superposed flow and the shear caused by the stationary casing. Axisymmetric, steady flow computations, using a low-Reynolds-number k-ε turbulence model, are not able to predict this flow structure accurately. Some qualitative features of the measured flows are reproduced, but velocity magnitudes tend to be overpredicted. There are some uncertainties surrounding inlet conditions for the flow entering the system through holes at the periphery of one of the rotating discs, however these uncertainties are not wholly responsible for the poor level of agreement between the computations and the data.

(ii) tangential velocity measurements confirm that the flow structure is determined mainly by the value of the turbulent flow parameter, λ_T, as suggested by a previous parametric study carried out computationally.

(iii) despite significant differences between measured and computed flow structures, Nusselt numbers for the heated upstream disc are in general reasonably well-predicted (provided that uncertainties in thermal boundary conditions for the system are taken into account), and the measured increase in heat transfer rate with both rotational Reynolds number and flow rate is reproduced adequately by the computations.

ACKNOWLEDGMENTS

The authors wish to thank BMW-Rolls-Royce GmbH, for funding the experimental research described in this paper, and Universiti Putra Malaysia, Malaysia, for providing the financial support for Mr Abdul Aziz Jaafar.

REFERENCES

Gan, X., Kilic, M. and Owen, J.M. 1994. Superposed flow between two discs contra-rotating at differential speeds, Int. J. Heat and Fluid Flow, 15, 438-446

Gan, X., Mirzaee, I., Owen, J.M., Rees, D.A.S. and Wilson, M. 1996. Flow in a rotating cavity with a peripheral inlet and outlet of cooling air, ASME Paper 96-GT-309

Herrero, J., Giralt, F. and Humphrey, J.A.C. 1999. Influence of the geometry on the structure of the flow between a pair of corotating discs. Phys. Fluids, 11, 86-96

Launder, B.E. and Sharma, B.I. 1974. Application of the energy dissipation model of turbulence to flow near a spinning disc, Letters in Heat and Mass Transfer, 1, 131-138

Mirzaee, I., Gan, X., Wilson, M. and Owen, J.M. 1998. Heat transfer in a rotating cavity with a peripheral inflow and outflow of cooling air, J. Turbomachinery, 120, 818-823

Mirzaee, I., Quinn, P., Wilson, M. and Owen, J.M. 1999. Heat transfer in a rotating cavity with a stationary stepped casing , J. Turbomachinery, 121, 281-287

Owen, J.M. and Rogers, R.H. 1995. Flow and heat transfer in rotating disc systems: Vol. 2, Rotating cavities, Research Studies Press, Taunton, UK and John Wiley, NY, USA

